# scientific reports

OPEN

# Integrated multi-analytical screening approach for reliable radiocarbon dating of ancient mortars

Giulia Ricci[1,2✉], Michele Secco[2,3], Anna Addis[4], Anna Pistilli[1], Nereo Preto[1], Gian Pietro Brogiolo[3], Alexandra Chavarria Arnau[3], Fabio Marzaioli[5], Isabella Passariello[5], Filippo Terrasi[5] & Gilberto Artioli[1,2]

Radiocarbon dating of the carbonate binder of historical mortars is a strategic research topic not lacking in complexities. The critical step is the separation of anthropogenic CaCO$_3$-binder from other carbonate sources that could severely affect the resulting dates. Here we present a complete procedure for the processing and characterization of difficult mortars and of the separated binder fractions in order to assess a priori the chances of positively dating the mortar, and produce a binder fraction yielding the most reliable radiocarbon dates possible. Two complex architectural case studies from Northern Italy are presented and discussed in detail: the churches of Santa Maria Maggiore (Lomello, Pavia) and Santa Maria (Torba, Varese). The results support that both the reliability assessment and the successful radiocarbon dating are possible through a multi-analytical approach encompassing mineralogical and petrographic characterization, X-ray powder diffraction, scanning electron microscopy, measurement of carbon and oxygen stable isotopes, and optical cathodoluminescence.

Radiocarbon dating ($^{14}$C) of archaeological and historical buildings is mostly based on dating organic materials. In the last 60 years, the possibility of using mortar as a material indicating the construction date of a building has been investigated, and there are examples of mortar dating studies that improved the chronological characterization of their investigated historical events[1,2]. Mortar-based materials are undoubtedly contemporary to the building and their methods of production make them valuable objects for radiocarbon dating a building's time of construction[3,4]. $^{14}$C on mortars exploits the uptake of atmospheric CO$_2$ by reaction with lime putty; atmospheric carbon is then stored into CaCO$_3$-binder during the carbonation process. This process makes mortars suitable for radiocarbon dating, since $^{14}$C is fixed into the carbonate binder[5–7].

Even if the method is conceptually simple, problems in the correct age estimation are common and are often related to the separation and selection of the pure binder fraction avoiding contaminants. The most common contaminants are: (i) geologic or fossil carbonate and lumps of original limestone, which affect the dating by incorporating dead carbon and severely overestimating the age. These components are generally defined as geogenic carbonate; (ii) secondary alteration processes, delayed hydraulic reactions and formation of long-term phases containing carbonate, which could be responsible of an underestimation of the age[8–11]. Large efforts were devoted by the scientists to find an efficient binder isolation method and control, but more dedicated studies in this peculiar field are still needed[12,13].

In this framework, we present our approach in dating mortars which is based on the significance of a complete characterization of the studied samples. An appropriate chemical and mineralogical characterization of both mortar and isolated binder greatly enhances the understanding of the material's features, allowing a preliminary assessment of the reliability of the binder for radiocarbon dating, and afterwards, the choice of the pre-treatments

[1]Department of Geosciences, University of Padova, Via Giovanni Gradenigo 6, 35131 Padua, Italy. [2]Inter-Departmental Research Centre for the Study of Cement Materials and Hydraulic Binders (CIRCe), University of Padova, Via Giovanni Gradenigo 6, 35131 Padua, Italy. [3]Department of Cultural Heritage (DBC), University of Padova, Piazza Capitaniato 7, 35139 Padua, Italy. [4]Bruker Italia S.R.L. Daltonics Division, Via Cluentina 26/R, 62010 Macerata, Italy. [5]Centre for Isotopic Research on Cultural and Environmental Heritage (CIRCE), University of Campania "Luigi Vanvitelli", Viale Carlo III 153, San Nicola La Strada, 81020 Caserta, Italy. ✉email: giulia.ricci@unipd.it

to be applied. Our approach includes, in brief: (i) a multi-analytical characterization of the material, in order to evaluate the crystal-chemical evolution of the sample and to identify potential dating contaminants; (ii) a careful binder extraction and processing in order to separate/eliminate the aggregate contaminants; (iii) a characterization of the extracted binder to check for the successful purification treatment; (iv) radiocarbon dating of the purified fraction.

In this research paper, mortar samples from two different archaeological sites in the north-western Italian region Lombardy are presented and discussed. Beside mortars, radiocarbon dating of lime lumps was also considered as may provide an alternative in radiocarbon dating, due to the carbonation process of calcium hydroxide contained in lime putty. In the same manner as the mortar matrix, the atmospheric $CO_2$ is fixed in the lumps to form calcium carbonate[8,14–16].

The aim is to evaluate the effectiveness of both the binder separation procedures and, in particular, the isotopic analyses (stable carbon and oxygen isotopes) as complementary method in evaluating the suitability of a given sample for radiocarbon dating. The characterization of the isolated binder fraction should be preliminary with respect to the radiocarbon dating analysis in order to ensure the complete removal of the contaminants. In this step, different complementary techniques were used since results obtained by one technique alone may be often controversial or partial.

In this research work, X-ray powder diffraction (XRPD), optical cathodoluminescence (OM-CL) and stable carbon and oxygen isotopes analysis ($\delta^{13}C$ and $\delta^{18}O$) were used together for the first time as complementary techniques in order to predict and select reliable candidates for radiocarbon dating. Moreover, capability and limits of each methods are evaluated and discussed.

X-ray powder diffraction (XRPD) is a powerful technique able to detect mineralogical phases resulting from pozzolanic reactions (C–S–H, AFm, M-S–H), delayed hydraulic reactions and newly formed phases containing carbonate formed over a relatively long period (LDHs), that could be responsible of an underestimation of the age[17–19]. LDHs, as hydrotalcite-like minerals, are mixed hydroxides with lamellar structure in which $M^{3+}$ cations partially substitute for $M^{2+}$ cations and the positive charge is balanced by anions (often carbonate) and water molecules arranged in interlayers in alternation with the octahedral layers[20,21]. The flexible layered structure favours dynamic exchanges of carbonate derived from atmospheric $CO_2$ even under ambient conditions[22–24], introducing recent carbon as contaminant in radiocarbon dating[11,25].

Optical-cathodoluminescence (OM-CL) exploits the luminescence properties of crystals when irradiated by an electron beam. Luminescence studies have long been used by geologists in order to investigate the provenance, minerogenesis, sediment source, diagenesis and cementation history of different kind of rocks and minerals[26,27]. In minerals, the luminescence response depends on intrinsic (lattice defects) and extrinsic (trace elements) point defects[28]. OM-CL has been one of the main screening methods for the identification of geogenic $CaCO_3$ aggregates in mortars. Observing the luminescence of varying colours emitted by grains of $CaCO_3$, it may be possible to discriminate geogenic carbonates (contaminants) from anthropogenic carbonates of binders. Most geogenic forms of $CaCO_3$, e.g., limestone, exhibit orange-red luminescence caused by the occurrence of $Mn^{++}$ in the calcite crystal lattice. Anthropogenic $CaCO_3$ shows instead dull luminescence, due to the $Mn^{++}/Fe^{++}$ ratio in the calcite related to the changing of Eh and pH conditions in the setting mortars[8,29–33]. When using cathodoluminescence to identify the absence of geogenic carbonates, there is an implicit assumption of geogenic carbonates being luminescent. This assumption is often justifiable, as limestones (generally used in mortar mixing) are almost always luminescent due to the $Mn^{++}$ incorporation to the crystal structure[30,31].

Finally, stable isotope analysis was used to test the nature of the carbonate phase due to the isotope fractionation of $\delta^{13}C$ and $\delta^{18}O$ isotopes during portlandite carbonation[34–40]. The stable carbon isotopes were exploited in order to differentiate the anthropogenic calcite versus any contamination. The ideal $\delta^{13}C$ value of a binder carbonate, formed by the atmospheric $CO_2$ absorption from calcium hydroxide, is between −27 and −20‰ VPDB[41]. In fact, variations from the ideal $\delta^{13}C$ to more positive or negative values may indicate the presence of contaminants (geogenic carbonate, layered phases containing recent atmospheric $CO_2$, etc.) that could invalidate the radiocarbon dating. The method has been extensively tested here, so that a detailed discussion of its applicability is provided.

### $\delta^{13}C$ and $\delta^{18}O$ isotopes analysis.

The stable isotope fractionation of carbon and oxygen in mortars depends on the manufacture and hardening processes, especially on the isotopic content of the atmospheric $CO_2$, the water present during the carbonation reaction, and the quality and quantity of the aggregates[42].

The $CaCO_3$-binder produced by carbonation process is identical in chemical composition to calcite produced at ambient temperature, however, the stable isotopic composition of anthropogenic as well as biogenic calcites may preserve information of the environment and conditions under which they were formed[41,43].

According to the literature and experimental data[35–37,44–46], the carbonate from lime mortar and/or cement and concrete forms under non-isotopic equilibrium conditions. The strong alkaline environment (pH > 11) and the consequent rapid absorption of $CO_2$ directly from the atmosphere induce the formation of calcite with an extreme isotopic composition[36,44]. In strong alkaline conditions it is estimated that 2/3 of $\delta^{18}O$ derives from the $CO_2$ and 1/3 from $OH^-$[41,47]. The isotope values are expressed relative to the VPDB-standard (Vienna Pee Dee Belemnite)[48].

Ideally, $\delta^{13}C$ and $\delta^{18}O$ of a lime-based binder formed by the carbonation reaction thorough direct absorption of atmospheric $CO_2$, in a strong alkaline environment (pH > 11), are $\delta^{13}C_{matrix} = -25$‰ (or −20.7‰ according to[42]) and $\delta^{18}O_{matrix} = -20$‰VPDB. According to[41,49,50], the ideal stable isotopes values of calcite formed directly by absorption of atmospheric $CO_2$ are: $\delta^{13}C_{calcite}$ between −27 and −20‰, and $\delta^{18}O_{calcite} = -19$‰. Such values best confirm that the $CO_2$ incorporated in the carbonate derives from the atmosphere[41,51] and therefore the isotopic ratios of the binder fraction are highly indicative of the purity of the binder, i.e., its anthropogenic nature[4,37,41].

| Site | Sample code | Sampling area | Construction phase |
|---|---|---|---|
| LOMELLO | LOM_1 | Baptistery of Saint Giovanni ad Fontes, basis of the baptismal font | V-VI sec. AD |
| | LOM_2 | Baptistery of Saint Giovanni ad Fontes, second baptismal font | VII-VIII sec. AD |
| | LOM_3 | Church of Santa Maria Maggiore, South-west wall of the basement | V-VI century A.D. (oldest phase of the church) or X-XI? |
| | LOM_4 | Church of Santa Maria Maggiore, South-west wall of the basement | V-VI century A.D. (oldest phase of the church) or X-XI? |
| | LOM_5 | crypt, above the column | X–XI sec. AD (?) |
| | LOM_6 | crypt, above the pulvinus of the column at the entrance | X–XI sec. AD (?) |
| | LOM_7 | crypt, joint between the capital and the pulvinus of the same column as LOM-6 | X–XI sec. AD (?) |
| TORBA (Castel Seprio) | TOR_1 | Church, inside the bell tower | Before or after the crypt? |
| | TOR_2 | Church, masonry in the corner | Before or after the crypt? |
| | TOR_3 | Crypt, plaster on the lower part | I crypt–VII–VIII sec. AD |
| | TOR_4 | Crypt, plaster on the upper part | I crypt–VII–VIII sec. AD |
| | TOR_5 | Crypt, reconstruction of the apse, lower part | Later than I–X–XI sec. AD |
| | TOR_6 | Crypt, reconstruction of the apse | Later than I–X–XI sec. AD |
| | TOR_7 | Crypt, upper part, external perimeter area of the church | II crypt–VII–VIII sec. AD |
| | TOR_9 | Buttress | III crypt |
| | TOR_10 | Crypt | Later than II–VII–VIII sec. AD |
| | TOR_12 | Building IV | Settlement IX–X sec. AD |
| | TOR_13 | Roman walls | V sec. AD |
| | TOR_14 | Tower | IX–X sec. AD |
| | TOR_15 | Wall behind the church | Late mediaeval period |
| | TOR_16 | Wall behind the church | Late mediaeval period |

**Table 1.** Mortar samples collected from the Lomello and Torba sites. The reported dates of the construction phases are those inferred from archaeological and historical information.

Marzaioli et al.[4], measured a similar range for $\delta^{13}$C of synthetic mortars (from −14.9 to −21.9‰) by calcination of a natural carbonate ($\delta^{13}$C = 2.9‰) and successive carbonation with natural air of the laboratory ($\delta^{13}$C = −11‰).

Indeed, variations from the ideal values of $\delta^{13}$C and $\delta^{18}$O towards positive or negative values indicate the presence of contaminants (such as geological carbonate, or newly formed phases that absorbed recent atmospheric $CO_2$) that can affect the $^{14}$C dating results. In most cases, the calcite matrix can be easily distinguished from limestone aggregates (e.g., marine limestone, dolomite, marble etc.) by their isotope values. Therefore, stable isotope analysis is potentially a powerful sample screening method for $^{14}$C dating.

In Supplementary Figure S1 (modified from[36]), the ideal binder values (IBV) and the variations of the isotopic ratios related to the calcite formation conditions are reported. The variations of the isotopic values according to lines 1–4 indicate the different types of alteration mechanisms potentially present in the sample. Line 1 indicates a binder geologically contaminated by the presence of limestone (line 1a and 1b are deviations due to relicts of limestone used for burning or contamination by limestone aggregates); line 2 indicates variability in water or rainwater, as heavy sources and/or evaporation effect; line 3 indicates that organic carbon contaminants may be present in the binder, fed carbon to the primary $CO_2$, or it may derive from biogenic alteration of anthropogenic calcite; line 4 indicates a variation due to either a primary source of $CO_2$ with light oxygen, or exchange with water derived from a light-oxygen source.

**Archaeological contexts and mortar samples.** The mortars investigated in the present work (see Table 1) were sampled from two different Lombard churches: Santa Maria Maggiore in Lomello (province of Pavia, coordinates 45.122594, 8.793882) and Santa Maria in the Abbazia di Torba complex (province of Varese, coordinates 45.729522, 8.863244).

The sampling was carried out considering the sampling depth in order to account the delayed carbonation problem, as discussed by Lindroos et al.[52], hence, were collected and analysed unaltered samples coming from the surface and not from deeper parts.

The sites were singled out for their historical and archaeological importance, despite of their very complex architectural developments. The mortars were carefully selected during archaeological excavations, on the account of their significance in the reconstruction and interpretation of the architectural sequence. The nature and features of the mortars proved to be a challenge for dating methods[38] and actually stimulated the present investigation in order to develop more efficient purification protocols and reliability tests, such as the $\delta^{13}$C analysis used to verify the purity-grade of the extracted fine binder fractions.

The church of Santa Maria Maggiore in Lomello, reconstructed in the year 1025 AD, is one of the most representative architectonic examples of First Romanesque art[53–55]. The church is part of a complex with an older baptistery, San Giovanni ad Fontes, built between the V and VIII century[56,57]. The mortar sampling was carried out into the baptistery (LOM_1 and LOM_2), southern wall of the church (LOM_3 and LOM_4) and the crypt (LOM_5, LOM_6 and LOM_7), as shown in Fig. 1A. Lime lumps (P) were also collected from three mortar samples (LOM_2, LOM_3 and LOM_4), characterized and dated by $^{14}$C.

**A) Church of Santa Maria Maggiore at Lomello**
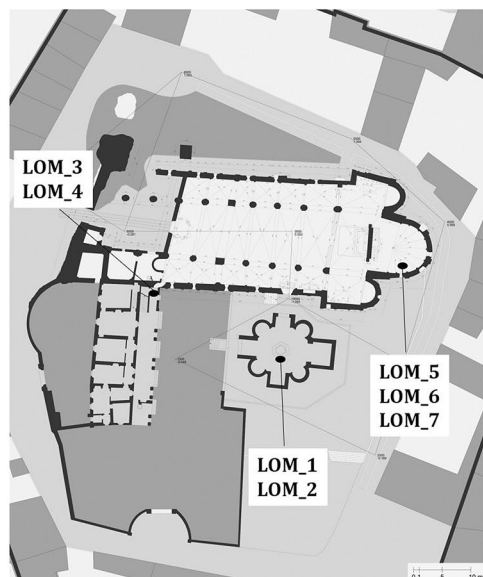
**B) Church and settlement of Torba**



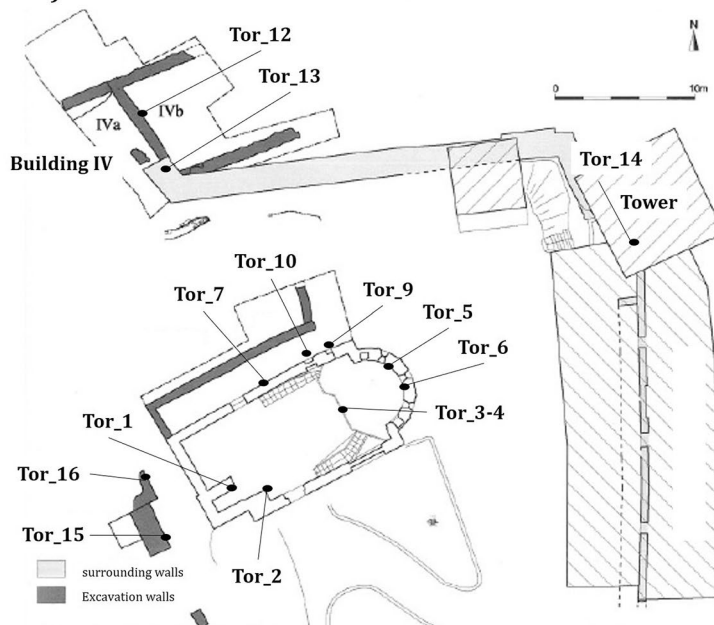**Figure 1.** Maps of the two archaeological sites with indication of the collected mortar samples. (GIMP 2.10.10. GNU Image Manipulation Program, https://www.gimp.org/). (**A**) The church of Santa Maria Maggiore at Lomello (Pavia) and (**B**) the church of Santa Maria and the settlement of Torba complex (Castelseprio, Varese).

The Torba site was funded as a military structure at the end of the IV or beginning of the V century, as a part of the Castel Seprio late roman fortification, and it was later (possibly from the VIII century) reused as a part of a Benedictine monastery consisting in a tower with a funerary floor and chapel, monastic spaces, a house (named building IV) hosting the non-religious members of the community (called *conversi*), and the church of Santa Maria. Recent analysis have defined four periods of evolution of the church (A, B, C, D), not totally clear[58,59]. During an excavation conducted in 2013–2014, a total of 14 mortar fragments were selected (Fig. 1B) and sampled from: the crypt of the church (TOR_1-7, TOR_9-10); the *so-called* Building IV, NW of the church (TOR_12); the Roman wall (TOR_13); the second floor of the tower NE of the church (TOR_14); the wall SW behind the church (TOR_15 and TOR_16). In addition, three lime lumps (P) manually collected from three mortar samples (TOR_7_P, TOR_10_P and TOR_12_P) were tested and radiocarbon dated.

## Results

**Mortars characterization.** The samples from the baptismal baths (LOM_1 and LOM_2) in the Baptistery of Saint Giovanni at Lomello, are macroscopically characterized by the presence of coarse-grained ceramic fragments used as aggregates. Under the optical microscope (Fig. 2), the matrixes present calcite interference colours, indicating the occurrence of carbonated lime binder. The large fragments of ceramic used as aggregates embed different types of inclusions, such as quartz and feldspars. Furthermore, limestone inclusions with the typical red/orange luminescence were observed by OM-CL (Fig. 2A), which may represent a potential problem in $^{14}C$ dating because they could produce radiocarbon ages older than the mortars. The XRPD analysis (see Supplementary Table S1) of these two samples indicates that the mortars are basically composed by c.a. 30%wt of calcite, ascribable to both the binder and the limestone inclusions, 30%wt of quartz and feldspars, related to the aggregates, and c.a. 35%wt of clay minerals and amorphous phases, related to the ceramic aggregates. The collected mortars from the church at Lomello (LOM_3-7) are characterized by a calcic binder and silicate-based rock aggregates, such as quartzites, schists, serpentinites and amphibolites. The mortars of the crypt (LOM_5-7) are undoubtedly related to the foundational structures of the church, the binder/aggregate ratio is very low and mineralogical characterization carried out by XRPD on the bulk samples shows low amount of calcite between 4 and 13%wt (Supplementary Table S1).

The 14 mortar samples collected from the archaeological site of Torba are characterized by homogenous structural and compositional features, poor cohesion and by the occurrence of coarse aggregates. Microscopically (Fig. 2C and D), the binder matrixes present a microcrystalline texture of carbonate composition, sometimes associated with clay fractions dispersed homogeneously in the matrix. Quartz, feldspars, amphiboles, micas (muscovite and biotite), flint and fragments of metamorphic rocks such as schists and quartzites are present as aggregates. Lime lumps were identified in all samples by both OM and SEM observations. Three of them were manually isolated and collected from the bulk samples TOR_7, TOR_10 and TOR_12, and analysed by XRPD, OM-CL, isotope ratios and finally they were radiocarbon dated. Under OM-CL, carbonate aggregates are identified as luminescent centres in the matrixes, which generally show low-medium luminescence and therefore are prone to efficient separation of the binder.
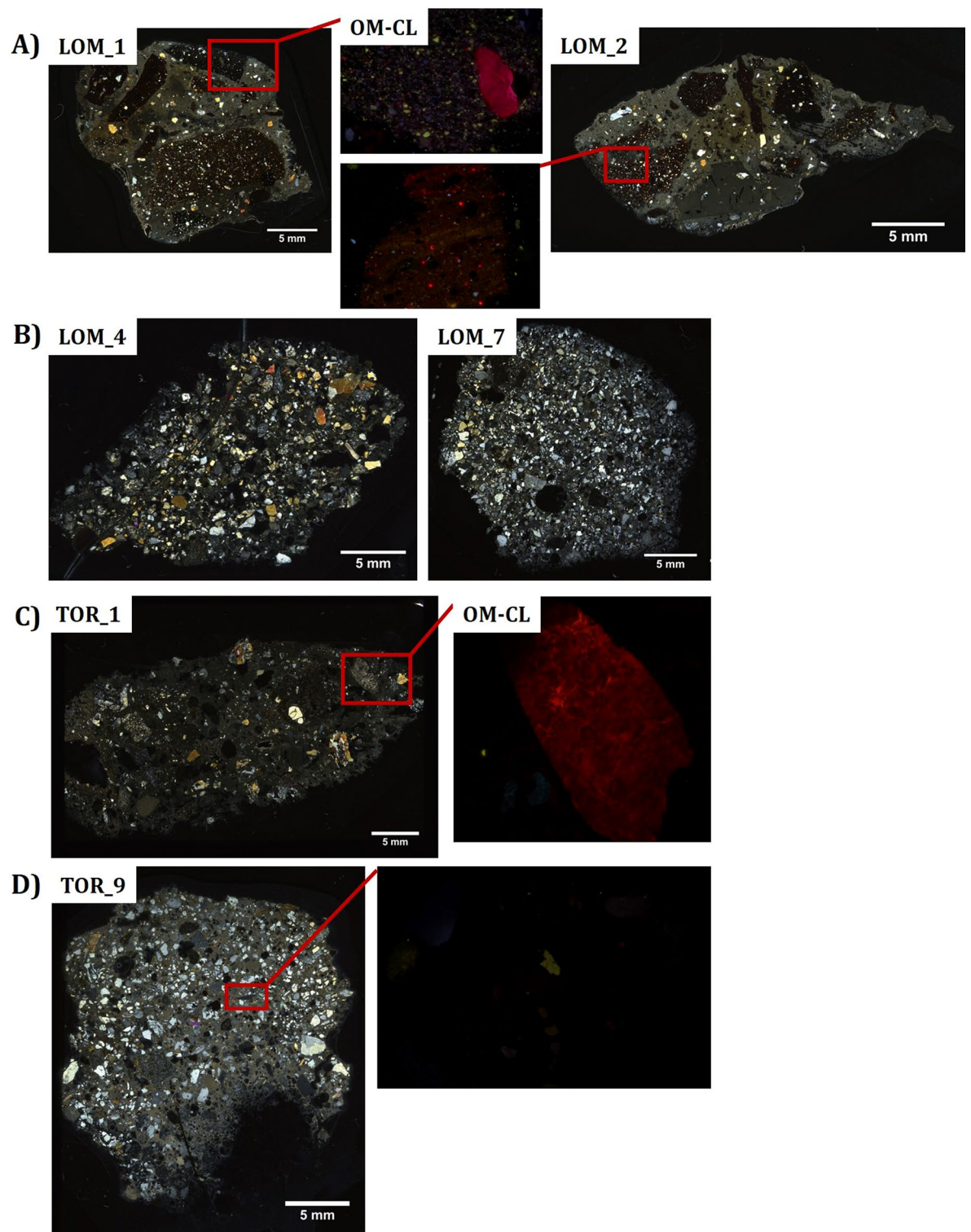
**Figure 2.** Representative mortar samples from Lomello and Torba under optical microscope in transmitted light. (**A**) polarized light micrographs of LOM_1 and LOM_2 thin sections (crossed polars), and OM-CL photos of the highlighted red squares; (**B**) polarized light micrographs of LOM_4 and LOM_7 thin sections (crossed polars). Polarized light micrographs of TOR_1 (**C**) and TOR_9 (**D**) thin sections (crossed polars), and OM-CL photos of the highlighted red squares.

Mineralogical investigation of the bulk samples, carried out by XRPD (Supplementary Table S1), shows the presence of quartz, albite, microcline, muscovite and amphiboles ascribable to the rock aggregates of the
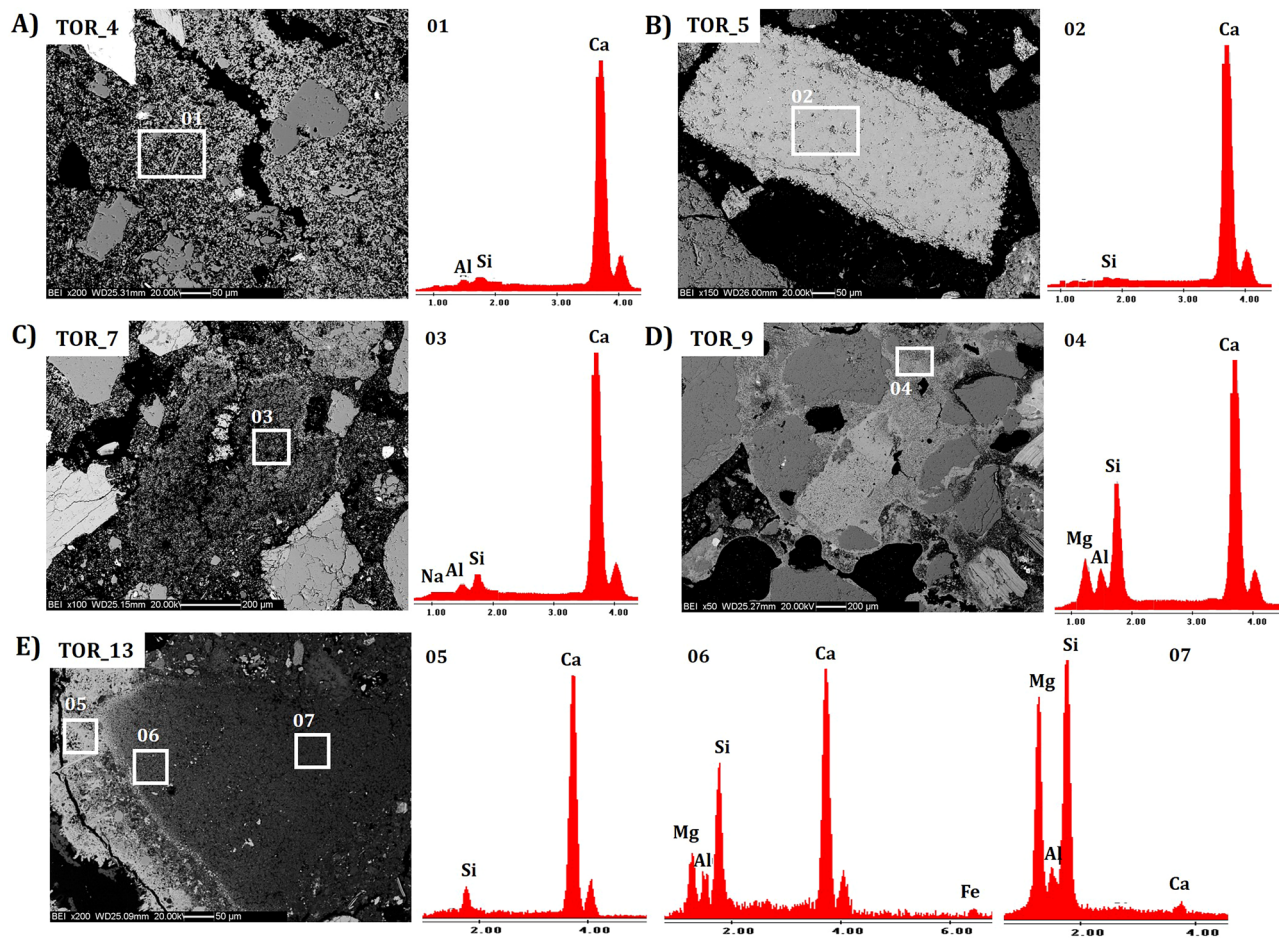
**Figure 3.** SEM–EDS microphotographs and elemental analyses of characteristic samples from Torba. (**A**) TOR_4, EDS microanalysis of the carbonate binding matrix (01); (**B**) image and microanalysis of a lump (02) within TOR_5; (**C**) TOR_7, microanalysis of the binding matrix (03); (**D**) TOR_9, microanalysis of the binding matrix (04); (**E**) TOR_13 microanalyses of a hydraulic lump (06, 07) and its rim (05).

mortar, as seen by OM observations. This composition may be related to the use of local sand[60]. The occurrence of phyllosilicates (as chlorite) may be related to a silty fraction added to the lime mixture, probably related to an inaccurate purification of the aggregate prior to mortar mixing[61]. The presence of calcite (up to 33 wt%) is attributed to both the aerial reaction of the binder fraction and the presence of carbonate aggregates as seen by optical microscopy. Substantial content of amorphous phases (between 7 to 28 wt%) may be related to the occurrence in the binding matrices of paracrystalline phases, possibly related to long term products of pozzolanic-type reactions. Indeed, the XRPD analysis highlights the occurrence in few samples (TOR_2, TOR_9, TOR_14) of double layered hydroxides (LDH). The presence of these hydrotalcite-type compounds may be due to the interaction between lime and reactive silicate aggregates such as Mg-rich phyllosilicates (chlorite)[11,24,25]. Generally, the mortar samples from Torba present a mineralogical composition ascribable to aerial mortars obtained by a lime binder and silicate sand. However, a few samples such as TOR_10, TOR_12, TOR_13 and TOR_15, are characterized by a mixture mainly composed of sand and clayey soil, with the addition of a small quantity of lime, as they are characterized by low content of calcite and higher amounts of amorphous, chlorite and silicate phases. The amorphous content may indicate the presence of paracrystalline phases related to hydraulic reaction products such as C-S-H, AFm and M-S-H phases[19]. SEM–EDS results are consistent with those obtained by XRPD. The matrixes present microcrystalline texture, evidences of calcic lumps and, in almost all the samples, a homogenous composition mostly composed by Ca (Fig. 3A and B). TOR_7, TOR_9 and TOR_16 mainly present matrixes with carbonate composition associated with portions characterized by significantly higher Si, Al and Mg concentrations, whereas the lumps' microanalyses suggest the use of a calcic binder (Fig. 3C and D). TOR_13 shows features indicative of a partial carbonation, heterogenous matrix mostly composed by Ca, Si, Al and Mg with lumps characterized by similar composition and microstructure (Fig. 3E). Generally, the presence of Si, Al and Mg in the binder matrixes may indicate the formation of hydrated magnesium silico-aluminate phases (M-A-S-H) after reaction between the lime binder and Mg-rich phyllosilicates (or other reactive silicates) of the aggregate fraction[19,62,63]. This is confirmed by the exceptional evidence of Mg-Si-Al-rich lumps in TOR_13, indicating pozzolanic reactions and the unusual formation of almost pure M-A-S-H lumps (Fig. 3E).

| Sample code | Fraction | Mineral phases | δ¹³C (‰) | δ¹⁸O (‰) | Luminescence |
|---|---|---|---|---|---|
| LOM_1 | Binder (SG) | ++Cc, --LDH, --Qtz | −21.1 | −15.5 | 0 |
| LOM_2 |  | ++Cc, -Clay | −21.4 | −15.3 | 0 |
| LOM_3 |  | +Cc, ++Arg, --LDH | −21.2 | −12.1 | 0 |
| LOM_4 |  | ++Cc, -Clay, -Arg, --Qtz | −23.6 | −17.3 | 0 |
| LOM_7 |  | ++Cc, -Arg, (t)Dol | −21.4 | −15.8 | 0 |
| LOM_2 | Lump (P) | ++Cc, -Qtz | −17.3 | −11.2 | 3 |
| LOM_3 |  | ++Cc, -Arg, (t)Qtz | −9.0 | −9.4 | 3 |
| LOM_4 |  | ++Cc, -Qtz | −18.5 | −17.9 | 3 |
| TOR_1 | Binder (SG) | ++Cc, -Dol, --Clay, --Qtz | −15.1 | −13.6 | 3 |
| TOR_2 |  | +Cc, +Dol, -Clay, -LDH, --Qtz | −13.3 | −11.4 | 3 |
| TOR_3 |  | ++Cc, -LDH, --Qtz | −11.6 | −19.4 | 0 |
| TOR_4 |  | ++Cc, --Qtz | −13.6 | −17.9 | 0 |
| TOR_5 |  | Cc, -Clay, --Arg, (t) LDH | −14.6 | −15.6 | 3 |
| TOR_6 |  | ++Cc, -Qtz | −19.8 | −15.0 | 0 |
| TOR_7 |  | ++Cc, --Qtz, (t)Clay | −16.7 | −16.9 | 0 |
| TOR_9 |  | ++Cc, --Qtz, (t) LDH | −9.2 | −14.7 | 1 |
| TOR_10 |  | ++Cc, --Qtz, (t) LDH | −17.5 | −17.3 | 0 |
| TOR_12 |  | ++Cc, --Qtz, --Arg | −16.7 | −13.1 | 0 |
| TOR_13 |  | Clay, M-A-S-H, --Cc | −12.2* | −21.9* | 0 |
| TOR_14 |  | ++Cc, -Clay, --LDH, --Qtz | −11.7 | −12.7 | 2 |
| TOR_15 |  | +Cc, +Clay, +LDH, M-A-S-H | −11.0 | −12.2 | 1 |
| TOR_7 | Lump (P) | ++Cc | −12.9 | −20.0 | 2 |
| TOR_10 |  | ++Cc | −6.9 | −18.1 | 0 |
| TOR_12 |  | ++Cc, -Arg | −17.1 | −9.8 | 0 |

**Table 2.** Summary table of the characterization carried on the binder fractions and lumps of the selected samples. Mineralogical phases (by XRPD), stable isotopes, and luminescence (by OM-CL) characterization results of the binder separate (SG) and lump (P) samples of the Lomello and Torba mortars are presented. Cc = calcite; Dol = dolomite; LDH = layer double hydroxides; Qtz = quartz; Arg = aragonite; M-A-S–H = hydrated magnesium-silicoaluminate phases (more details are provided in the supplementary material). (++) very abundant, (+) abundant, (-) scarce, (--) very scarce, (t) trace. 0 = dull, 1 = low, 2 = low-medium, 3 = medium-bright, 4 = bright. *very low signal of carbon.

**Characterization of the binder fractions (SG) and lumps (P).** Representative mortar samples collected from both Lomello and Torba were subject to the separation procedure in order to separate the binder fraction (SG) from the contaminants and aggregates. The SGs were then characterized by XRPD, OM-CL and stable isotope analyses. The characterization of the separated binder fractions allows checking whether the samples are suitable for dating, to limit the number of samples to be dated and the relative costs, and to preliminary assess the possible causes of error.

Among the 7 mortar samples from Lomello, 5 samples were selected (LOM_1-4 and LOM_7) and subject to the purification procedure. As previously discussed, in these mortars the binder/aggregate ratio is very low, and consequently, the purification procedure was carried out very carefully to avoid loss of the scarce binder material. The LOM_SGs characterization indeed suggests that these SG fractions can reliably be used to date the construction time of the building. The δ¹³C values are between −23.6 and −21.1‰ (Table 2 and Fig. 4A), suggesting carbonate formation directly by absorption of atmospheric $CO_2$[35,41]. The δ¹⁸O values are between −17.3‰ (sample LOM_4_SG) and −12.1‰ (sample LOM_3_SG). As discussed in literature, the enrichment of heavier oxygen isotopes with respect to a typical anthropogenic mortar carbonate may depend on the primary water source and/or to the evaporation of water during the hardening process of the mortars. Furthermore, it has been observed that this enrichment may also be due to re-equilibration with the silicate minerals, especially in cases of low binder/aggregate ratio[41,50,64,65]. However, as shown in Fig. 4A, the selected mortar samples (SGs) lay in the area B mostly indicating a small contamination ascribable to the oxygen fractionation of altered calcite or the use of isotopically heavy water[36,41,50]. The XRPD results (Table 2) show a mineralogical composition almost entirely constituted of calcium carbonate, and no evidences of geological carbonate contaminations in CL observations are detected. The presence of aragonite (metastable polymorph of calcium carbonate) in some samples (both from Lomello and Torba) is ascribable to the carbonation process[66], since no evidence of shell fragments or other biogenic carbonates was observed during the characterization analyses. Therefore, these samples may be good candidates for the radiocarbon dating.

On the other hand, the collected lime lumps (LOM_2-4_Ps) are characterized by: a mineralogical composition mostly of calcite, more positive δ¹³C values between −18.5‰ and −9.0‰ (Table 2) and a bright red luminescence (Supplementary Figure S3A). These features are indicative of the presence of limestone residues which were incompletely calcined[63]. In particular, sample LOM_3_P show a significant shift to heavier isotopic values, likely
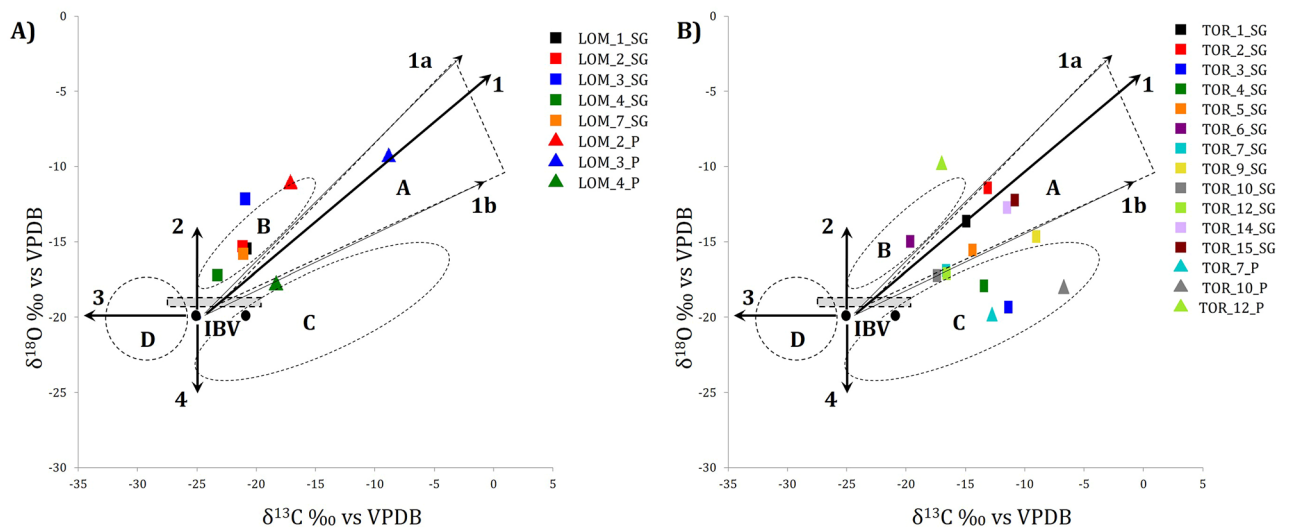
**Figure 4.** Isotopic ratios ($\delta^{13}C$ and $\delta^{18}O$) diagram of both mortar binders (SG) and lumps (P) of Lomello (**A**) and Torba (**B**). The IBV points (dark circles) and bars (gray dashed rectangle) represent the Ideal Binder Values. Trend lines (1–4) and marked areas (**A**–**D**) as reported in Supplementary Figure S1 and discussed in the introduction. Sample TOR_13_SG is not inserted in the diagram because its low carbon content yields unreliable results.

related to the isotopic signature of the limestone used for burning. LOM_2_P and LOM_4_P exhibit a milder shift towards heavier $\delta^{13}C$ isotope values, likely due to small impurities of isotopically heavy limestone, since luminescence investigation on powdered lumps show a medium-bright luminescence. Therefore, the Lomello lime lumps (Ps) may not be good candidates for radiocarbon analyses due to the systematic presence of geological carbonate contaminations.

Concerning the case study of Torba, almost all the mortar samples were selected for the separation and characterization procedures. The extracted binder fractions show different features. Most of them show a dull luminescence, proving the efficacy of the separation procedure; however, a higher $\delta^{13}C$ with respect to the ideal value IBV between −27 and −20‰ (VPDB) is observed, indicating some alteration and/or contamination of the mortar samples as the presence of other carbon sources, such as modern atmospheric carbon dioxide, secondary calcite and/or geological limestone[36,41,42]. SGs are mainly characterized by a mineralogical composition with high quantities of calcite and limited fractions of quartz, phyllosilicates (clays) and traces of LDHs. In TOR_1_SG and TOR_2_SG, dolomite is also present, probably due to the fine fraction of the dolomitic aggregate. Dolomite is also present in the bulk XRPD characterization. TOR_13_SG and TOR_15_SG show different mineralogical composition with less calcite, clays and presence of LDH phases. Furthermore, as suggested by SEM–EDS analyses, the mineralogical profiles observed by XRPD reported in Supplementary Figure S2 in the supplementary materials, are similar and attributable to those of M-S-H and M-A-S-H phases characterized by small particle size, low crystallinity and broad peaks of low diffracted intensity[67,68].

The samples TOR_1_SG, TOR_2_SG, TOR_5_SG and TOR_14_SG show diffuse luminescent centres and, in general, a medium-bright luminescence intensity, probably due to residues of carbonate aggregates. The stable isotopic composition of these 4 samples, $-15.1 < \delta^{13}C < -11.7$‰ and $-15.6 < \delta^{18}O < -11.4$‰ (Fig. 4B, Table 2), indicate that these mortars are affected by limestone contamination. TOR_6_SG, TOR_7_SG, TOR_10_SG and TOR_12_SG have $\delta^{13}C$ values between −19.8 and −16.7‰, dull luminescence, and mineralogical composition mostly of calcite, therefore these samples should be nearly free of contaminants.

TOR_3_SG and TOR_4_SG, with $\delta^{13}C$ equal to −11.6‰ and −13.6‰ respectively, dull luminescence and the presence of LDH phases (in the case of TOR_3_SG), exhibit minimal contamination from atmospheric $CO_2$ and recent $CO_2$ likely absorbed by carbonate-containing double layered hydroxides (LDHs)[25,41] and secondary phases.

The last two mortar samples, TOR_9_SG and TOR_15_SG, may be affected by different contaminations. The characterization shows dull luminescence and more positive isotopic values than the ideal ones. Furthermore, the XRPD results show the presence of calcite, low amount of quartz, clayey phases, LDHs and poorly crystalline phases such as M-A-S–H, particularly in TOR_15_SG. The enrichment of $\delta^{13}C$ may be related to slow continuous calcite formation and segregation of $^{12}C$ in the gas phase, and to the presence of isotopically heavy limestone impurities. Both calcite types may indeed have dull luminescence. High $\delta^{13}C$ isotope values may be expected in mortar mixes composed by small amounts of lime binder and large quantities of silicates prone to delayed pozzolanic reactions, as in the case of sample TOR_15[41,65].

Among the lime lump samples, TOR_7_P and TOR_10_P are characterized by white colour, mineralogical composition mainly composed of calcite, high $\delta^{13}C$ and $\delta^{18}O$ values, and dull luminescence. As in the case of the TOR_3_SG and TOR_4_SG, these lumps may present contamination due to precipitation of calcite formed from more recent atmospheric $CO_2$. It is possible that also TOR_7_P and TOR_10_P contain secondary calcite formed sometime after the main carbonation reaction of the binder mortars, thus causing an underestimation of the measured radiocarbon date[14,69]. TOR_12_P is characterized by an essentially carbonate composition, and

| CIRCE Code | Sample code | Area | Fraction | $^{14}$C age (BP) | Cal. age range (1σ) | Cal. age range (2σ) |
|---|---|---|---|---|---|---|
| DSH6797 | LOM_1 | Baptistery | Binder SG | 1525 ± 35 | AD 444–600 | AD 433–635 |
| DSH6989 | LOM_2 | Baptistery | | 1356 ± 37 | AD 645–759 | AD 605–775 |
| DSH6798 | LOM_3 | Church of Santa Maria Maggiore | | 1072 ± 27 | AD 900–1020 | AD 893–1025 |
| DSH6990 | LOM_4 | Church of Santa Maria Maggiore | | 877 ± 38 | AD 1054–1221 | AD 1043–1260 |
| DSH6799 | LOM_7 | Crypt | | 1059 ± 28 | AD 977–1024 | AD 895–1030 |
| DSH6781 | LOM_2 | Baptistery | Lump P | 1731 ± 38 | AD 253–383 | AD 245–408 |
| DSH6782 | LOM_3 | Church of Santa Maria Maggiore | | 18,181 ± 89 | BC 20,296–20,096 | BC 20,397–19,993 |
| DSH6783 | LOM_4 | Church of Santa Maria Maggiore | | 1415 ± 47 | AD 603–656 | AD 557–757 |
| DSH6771 | TOR_4 | Crypt | Binder SG | 1393 ± 33 | AD 609–662 | AD 596–675 |
| DSH6773 | TOR_7 | Church walls | | 1417 ± 35 | AD 605–653 | AD 582–664 |
| DSH6775 | TOR_10 | Church walls | | 1275 ± 31 | AD 680–770 | AD 663–824 |
| DSH5617 | TOR_15 | West wall behind the church | | 353 ± 30 | AD 1478–1626 | AD 1459–1635 |
| DSH6774 | TOR_7 | Church wall | Lump P | 1078 ± 28 | AD 902–1017 | AD 893–1024 |
| DSH6777 | TOR_10 | Church wall | | 988 ± 27 | AD 1021–1147 | AD 994–1155 |
| DSH6768 | TOR_12 | Building IV | | 1110 ± 32 | AD 895–989 | AD 776–1018 |

**Table 3.** Radiocarbon dating results.

no geogenic-related cathodoluminescence signal is observed. Its δ$^{13}$C value (−17.1‰) is close to the ideal values and the δ$^{18}$O value (−9.8‰) suggests a heavy isotopic composition of the water interacting with the binder during the carbonation process, or alteration after the hardening process of the mortar[50]. However, TOR_12_P may be considered as a reliable lump sample for radiocarbon dating.

**Radiocarbon dating.** The characterization carried on the separated binder fractions (SGs) and lumps (Ps) allowed to identify the suitable samples in order to date the construction phases of the archaeological sites. The choice of the samples for radiocarbon dating was made considering the archaeological relevance and the results obtained by XRPD, OM-CL and isotopic ratio of stable carbon isotopes δ$^{13}$C characterization. Furthermore, for the sake of testing our method, radiocarbon dating of predicted unreliable samples was also performed.

In the following table (Table 3), $^{14}$C results including radiocarbon ages and calibrated calendar ages of all the selected and analysed samples are presented.

The characterized mortar samples from Lomello (LOM_1-4_SGs and LOM_7_SG) were selected as good candidates for radiocarbon dating on the basis of their characterization, whereas the three lumps (LOM_2-4_Ps) present contaminations probably due to geological carbonates, detected by both stable isotopes and OM-CL characterization. All samples were nonetheless dated and the calibrated calendar ages were compared with those expected and discussed.

The two SG samples of the mortars collected from the Baptistery in Lomello (LOM_1-2_SG) show calibrated dates (AD 433–635 and AD 605–775, respectively) in agreement with the ages expected from historical and archaeological considerations (V-VI sec. AD and VII-VIII sec. AD, respectively). On the other hand, the calibrated age of the lump sample of the second bath (LOM_2_P, AD 245–408) is older than the mortar LOM_2 and consequently older than the expected date (VII-VIII sec. AD), as predicted by the characterization analyses showing that the sample is clearly contaminated by geological carbonate. Similar results are obtained for the samples related to the church and crypt of the Santa Maria Maggiore, where the SGs (LOM_3-4_SG and LOM_7_SG) show calibrated calendar ages (see Table 3) very close to the documented construction period of the church (X and XI century AD). Sample LOM_3_P, characterized by more positive δ$^{13}$C value and bright red luminescence, and sample LOM_4_P, with medium-bright luminescence, show unreliable old ages of c.a. 20,000 B.C. and c.a. 600 A.D, respectively, demonstrating that these samples are not reliable candidates for radiocarbon dating due to contamination of geological carbonates, according to experimental characterization.

Prioritizing good candidates for radiocarbon dating and their relevance for archaeological questions, TOR_4_SG, TOR_7_SG and TOR_10_SG were the selected samples of the crypt (TOR_4) and of the outer wall of the Santa Maria church of Torba (TOR_7 and TOR_10). The sample TOR_15_SG, from the west wall behind the church, was also selected for the testing procedure: it is characterized by the presence of LDHs, high δ$^{13}$C and δ$^{18}$O values and dull luminescence, indicating the presence of contaminants which should bias its radiocarbon age. The three lump samples were also dated.

Radiocarbon dating results (Table 3) of the TOR_7_SG and TOR_10_SG, selected as reliable samples for radiocarbon measurements, show calibrated calendar dates between 582 and 824 AD, which are correct according to archaeological hypotheses[58], where the assumption is that the constructions are older than the X century. Sample TOR_4_SG is radiocarbon dated to between 596 and 675 AD. Archaeological records temporally place the sample TOR_7 before TOR_10, while samples TOR_4 and TOR_7 belonging to the VII-VIII sec AD. The experimentally measured dates of TOR_4 and TOR_7 are essentially coeval, confirming the archaeological expectations. TOR_4_SG seemed to be slightly contaminated by recent carbon, as suggested by the isotope ratio measurements (δ$^{13}$C = −13.6). However, XRPD and CL investigations did not detect any LDH phases and/or re-precipitated calcium carbonate. Another possibility in having recent carbon contaminants can be a mortar affected by a delayed carbonation process[52]. TOR_4 was collected from the basement of the church, and, as well

as the other samples, the sampling was made considering the general problems related to delayed hardening in the sampling depth[52].

The calibrated calendar age obtained for the sample TOR_15_SG (AD 1459 − 1635) is too young. Archaeological studies predicted a late dating of this particular wall, however, the multi-analytical characterization allowed to identify different kind of contaminations in the sample that can lead to various uncertainties on the dating obtained. Stable isotopes results approach the isotopic composition of modern $CO_2$ ($\delta^{13}C$ between −9 and −6‰ (VPDB)[36]) suggesting the presence of contamination probably due to the LDH phases, detected by XRPD investigation, which incorporated $CO_2$ after the hardening process[11,25].

The calibrated age of lump sample TOR_12_P is correct (AD 776−1018), in accordance with the indications of its mineralogical and isotopic characterization. On the other hand, the dates obtained for lump samples TOR_10_P and TOR_7_P are sensibly younger than those of the SGs of the same samples, and are to be considered unreliable, as already suggested by isotopic analyses. The general indication is that lime lumps must be very carefully controlled before radiocarbon dating.

## Discussion and conclusions

The multi-analytical approach used for characterizing the binder fraction of mortars in two historical sites of Lombardy, i.e. Lomello and Torba, is a promising protocol for a pre-selection of suitable samples for radiocarbon dating. The novel application of the chosen techniques on extracted binder fractions show how their complementarity can be effective overcoming the limits of each single technique.

The radiocarbon ages of the SG samples selected by multi-analytical characterization are consistent with ages expected from archaeological, historical, and textual information. Lime lumps have been shown to frequently include under-burnt limestone cores that seriously affect the radiocarbon ages, as observed by CL-OM and stable isotopes results. The use of lime lumps in dating must therefore be exerted with caution.

From an archaeological point of view, the VII century date for Santa Maria di Torba introduces a new chronology for this type of simple hall crypt surmounted by vaults: it would precede those with a western corridor, built around the middle of the VIII century in Pavia (as Santa Maria alle Cacce and San Salvatore/San Felice) and in the territory of Brescia (San Salvatore di Sirmione and San Giorgio di Montichiari), until now considered the oldest in northern Italy[59].

In the church of Santa Maria di Lomello, stratigraphic analyses have identified the successive stages of the Romanesque construction. The dating of the mortars to around the year 1000 (compatible with the $1020 \pm 72$ thermoluminescence dating of a brick in the pilaster strip of the north perimeter, as reported in[70]) suggests that the church was built by Cunberto, the count of Lomello from 996, and his son Ottone, count of the palace and of Pavia from 999 to 1014.

The investigated case studies clearly demonstrate the importance of the mortar binder characterization by multiple techniques (isotopic signature, XRPD, and cathodoluminescence) to evaluate in detail the presence of possible contaminants and common biases affecting the radiocarbon measurements (Table 4).

Stable isotope analyses proved to be an effective tool to predict the unsuitability of a sample for $^{14}C$ dating, effectively recording contaminations. However, it has to be noted that the use of isotopic data alone would have led to exclude various samples due to an isotope ratio not exactly coincident with the range of the ideal binder, as suggested by the data reported in the literature[36] and reported in the supplementary materials of this article (Supplementary Figure S1).

The complementary techniques, such as XRPD and CL-OM used in the characterization procedures, fundamentally support the effectiveness of the separation procedure and considerably increase the chances of reliable dating. Integrating the obtained results, reliable samples can be chosen and radiocarbon dated. The XRPD analysis provides information on the mineralogical composition of the binder fraction identifying radiocarbon contaminants as LDHs, nevertheless, when calcite is identified as the major component of the binder fraction, this technique is not able to distinguish among geogenic, anthropogenic or secondary calcite. For this purpose, CL is generally applied in assessing the nature of the calcium carbonate, and the luminescence response caused by both geogenic and secondary calcite can be discussed with the isotopic values in order to better identify if it was an old or a young contamination.

It is proposed that the described protocol strengthen the whole procedure of radiocarbon mortar dating, based on solid experimental information.

## Materials and methods

**Analytical approach and methods.** The adopted analytical approach consists of the following strategy: (i) chemical–mineralogical characterization of the mortars; (ii) multi-step purification procedure of the mortar binders; (iii) characterization of the extracted purified binder fractions and evaluation of the reliability of the selected samples for radiocarbon dating; (iv) graphitization and radiocarbon dating of the purified fractions.

Besides mortar samples, selected lime lumps manually collected from the same mortar samples were characterized and radiocarbon dated.

Characterization and purification procedures were performed at the CIRCe Centre in Padua (Department of Geosciences, University of Padova, Italy), whereas graphitization and AMS measurements were carried out at CIRCE Centre in Caserta (Department of Mathematics and Physics, University of Campania, Italy).

**Chemical and mineralogical characterization.** The selected mortars were characterized by a multi-analytical approach aiming at assessing the nature of the binders and the presence of potential contaminants. Petrographic analyses were performed using a Nikon Eclipse ME600 optical microscope equipped with a Canon EOS 600D Digital camera on 30 µm thin-sections under parallel and crossed polars. Selected thin sections were

| Sample code | Area | Construction phase/expected age | Fraction | Radiocarbon contaminants? | ¹⁴C Cal. AD age range (2σ) | Reliable calibrated calendar age? |
|---|---|---|---|---|---|---|
| LOM_1 | Baptistery | V-VI sec. AD | SG | No | AD 433–635 | Yes |
| LOM_2 | Baptistery | VII-VIII sec. AD | SG | No | AD 605–775 | Yes |
| | | | P | Yes, geogenic carbonate | AD 245–408 | No (older) |
| LOM_3 | Church of Santa Maria Maggiore | V-VI century A.D. (oldest phase of the church) or X-XI? (?) | SG | No | AD 893–1025 | Yes |
| | | | P | Yes, geogenic carbonate | BC 20,397–19,993 | No (older) |
| LOM_4 | Church of Santa Maria Maggiore | V-VI century A.D. (oldest phase of the church) or X-XI? (?) | SG | No | AD 1043–1260 | Yes |
| | | | P | Yes, geogenic carbonate | AD 557–757 | No (older) |
| LOM_7 | Crypt | X-XI? (?) | SG | No | AD 895–1030 | Yes |
| TOR_4 | Crypt, plaster on the upper part | I crypt–VII–VIII | SG | No (?)* | AD 596–675 | Yes (?)* |
| TOR_7 | Crypt, external perimeter area of the church | II crypt–VII–VIII | SG | No | AD 582–664 | Yes |
| | | | P | Yes, recent CO₂ | AD 893–1024 | No (younger) |
| TOR_10 | Church walls, crypt | Later than II–VII–VIII | SG | No | AD 663–824 | Yes |
| | | | P | Yes, recent CO₂ | AD 994–1155 | No (younger) |
| TOR_12 | Building IV | IX–X sec. AD | P | No | AD 776–1018 | Yes |
| TOR_15 | West wall behind the church | Late medieval period | SG | Yes, geogenic carbonate and recent CO₂ | AD 1459–1635 | No (?) |

**Table 4.** Summary table. The expected and the calibrated calendar ages of the Lomello and Torba samples are reported and compared. *Isotope ratio measurements suggested TOR_4_SG to be slightly contaminated by recent carbon, however, XRPD and CL investigations did not detect any LDH phases and/or re-precipitated calcium carbonate. The date can be assumed to be correct.

observed under an optical cathodoluminescence microscope (OM-CL) in order to evaluate the presence of geogenic carbonates, using a petrographic microscope NIKON Labophot2-POL equipped with a cold cathode stage Cambridge Image Technology Ltd, CL8200 MK3 operated at a voltage of 15 kV and a current of 200 μA. Furthermore, thin sections covered with an ultrathin coating of graphite, were microstructurally and microchemically characterized through a CamScan MX2500 Scanning Electron Microscope (SEM) equipped with a LaB₆ electron source and an EDS used to collect elemental microanalyses (system resolution of 126.8 eV for 5.9 eV Mn) through the SEMQuant Phizaf software, giving valuable information on the mineral phases, binder composition and presence of hydraulic reactions. Mineralogical quantitative phase analyses (QPAs) were performed by XRPD on fine powders obtained from bulk samples by micronization. XRPD analyses were performed using a Malvern PANalytical X'Pert PRO diffractometer in Bragg–Brentano geometry, Co–Kα radiation, 40 kV and 40 mA, equipped with a real-time multiple strip (RTMS) detector (X'Celerator by Malvern Panalytical). Data acquisition was performed by operating a continuous scan in the range 3°–85° 2θ, with a virtual step scan of 0.02° 2θ. Diffraction patterns were interpreted with X'Pert HighScore Plus 3.0 software by Malvern PANalytical, reconstructing mineral profiles of the compounds by comparison with ICDD and ICSD diffraction databases. QPAs were performed using the Rietveld method[71] and refinements were accomplished using the TOPAS software (version 4.1) by Bruker AXS. The determination of both crystalline and amorphous content was calculated by means of the internal standard method with the addition of 20 wt% of zincite (ZnO) to the powders[72].

**Multi-step purification procedure.** The purification procedure of selected mortars was carried out in order to remove aggregates and potential dating contaminants by wet gravimetric sedimentation. The procedure consists in a sonication and wet gravimetric sedimentation in ultra-pure decarbonated water for 24 h, centrifugation and filtration of the fine fraction (labelled SG)[6,25,38,73]. The separation procedure needs between 15–30 g of mortars, and generally 10 to 100 mg of the fine fraction can be obtained depending on the ratio binder/aggregate.

**Characterization of the extracted fine binder and lime lumps.** The ultra-pure fine binder fractions (SGs) and the lime lumps (Ps) were characterized before radiocarbon dating in order to verify the absence of contaminants. The characterization included: XRPD, OM-CL and stable carbon and oxygen isotope analyses. The latter was carried on by a Thermo Scientific Delta V Advantage Isotope Ratio Mass Spectrometer. In details, about 0.6 mg of SGs were weighted in exetainer vials. $CO_2$ was developed at 70 °C by complete reaction with > 99% $H_3PO_4$ in a Gasbench II device connected to the spectrometer. Results were calibrated with two internal standards (sieved Carrara marble and Millipore Suprapur® carbonate), which are in turn periodically calibrated against the international reference carbonates NBS 19; NBS 18 and L-SVEC. A control standard (sieved Monzoni marble) was also run and treated equally to the samples and reproduced with external errors of better than 0.1‰ (1σ) for both carbon and oxygen. XRPD and OM-CL were applied to the separated binder fractions by adopting the same analytical protocols described above used for the bulk samples.

**Radiocarbon dating of the purified fractions and lumps.** The SGs and Ps were digested under vacuum by means of a complete orthophosphoric acid attack for 2 h at 80°C[4]. The released $CO_2$ was reduced to

11

graphite on iron powder catalyst according to the CIRCE sealed tube reaction protocol[74]. In details, IAEA C1 historical series (mass of carbon vs apparent age) were used for background correction and IAEA C2 was used for normalization purposes[4]. [14]C isotopic ratios were measured according to[75] and corrected for fractionation and blank, normalised and R.C. ages were estimated (M and H 1977) and calibrated to absolute ages by means of OxCal 4.4.4[76] and INTCAL20 calibration curve.

## Data availability
All data are available in the main text or the supplementary materials.

## References
1. Delibrias, G. & Labeyrie, J. Dating of old mortars by the carbon-14 method. *Nature* **201**, 742 (1964).
2. Folk, R. L. & Valastro, S. Successful technique for dating of lime mortar by carbon-14. *J. F. Archaeol.* **3**, 203–208 (1976).
3. Hale, J., Heinemeier, J., Lancaster, L., Lindroos, A. & Ringbom, A. Dating ancient mortar. *Am. Sci.* **91**, 130–137 (2003).
4. Marzaioli, F. *et al.* Mortar radiocarbon dating: Preliminary accuracy evaluation of a novel methodology. *Anal. Chem.* **83**, 2038–2045 (2011).
5. Heinemeier, J. *et al.* AMS 14C dating of lime mortar. *Nucl. Instrum. Methods Phys. Res. B* **123**, 487–495 (1997).
6. Nonni, S. *et al.* [14]C mortar dating: The case of the medieval Shayzar citadel, Syria. *Radiocarbon* **55**, 514–525 (2013).
7. Van Strydonck, M. Radiocarbon dating of lime mortars: A historic overview. In *4th Historic Mortars Conference - HMC 2016* 648–655 (2016).
8. Lindroos, A., Heinemeier, J., Ringbom, Å., Braskèn, M. & Sveinbjörnsdóttir, Á. Mortar dating using ams ^{14}C and sequential dissolution: examples from medieval, non-hydraulic lime mortars from the Aland Island, SW Finland. *Radiocarbon* **49**, 47–67 (2007).
9. Michalska, D. & Czernik, J. Carbonates in leaching reactions in context of 14C dating. *Nucl. Instrum. Methods Phys. Res. Sect. B Beam Interact. Mater. Atoms* **361**, 431–439 (2015).
10. Artioli, G. *Scientific Methods and Cultural Heritage* (Oxford University Press, 2010).
11. Ponce-Antón, G., Ortega, L. A., Zuluaga, M. C., Alonso-Olazabal, A. & Solaun, J. L. Hydrotalcite and hydrocalumite in mortar binders from the medieval castle of portilla (Álava, north Spain): Accurate mineralogical control to achieve more reliable chronological ages. *Minerals* **8**, 326 (2018).
12. Addis, A. *et al.* Selecting the most reliable ^{14}C dating material inside mortars: The origin of the Padua Cathedral. *Radiocarbon* **61**, 375–393 (2019).
13. Urbanová, P., Boaretto, E. & Artioli, G. The state-of-the-art of dating techniques applied to ancient mortars and binders: A review. *Radiocarbon* **62**, 503–525 (2020).
14. Pesce, G. *et al.* Radiocarbon dating of lumps from aerial lime mortars and plasters: Methodological issues and results from San Nicolò Of Capodimonte Church (Camogli, Genoa, Italy). *Radiocarbon* **51**, 867–872 (2009).
15. Pesce, G. L. A., Ball, R. J., Quarta, G. & Calcagnile, L. Identification, extraction, and preparation of reliable lime samples for ^{14}C dating of plasters and mortars with the "pure lime lumps" technique. *Radiocarbon* **54**, 933–942 (2012).
16. Pesce, G. L. & Ball, R. Radiocarbon dating of lime mortars. *J. Build. Limes Forum* **22**, 15–24 (2015).
17. Tian, J., Guo, Q., Tian, J. & Guo, Q. Thermal decomposition of hydrocalumite over a temperature range of 400–1500°C and its structure reconstruction in water. *J. Chem. J. Chem.* **2014**, 1–8 (2014).
18. Roelofs, J. C. A. A., van Bokhoven, J. A., van Dillen, A. J., Geus, J. W. & de Jong, K. P. The thermal decomposition of Mg-Al hydrotalcites: Effects of interlayer anions and characteristics of the final structure. *Chem. A Eur. J.* **8**, 5571–5579 (2002).
19. Secco, M. *et al.* Technological transfers in the Mediterranean on the verge of Romanization: Insights from the waterproofing renders of Nora (Sardinia, Italy). *J. Cult. Herit.* **44**, 63–82 (2020).
20. Pérez-Ramírez, J. & Abelló, S. Thermal decomposition of hydrotalcite-like compounds studied by a novel tapered element oscillating microbalance (TEOM). Comparison with TGA and DTA. *Thermochim. Acta* **444**, 75–82 (2006).
21. Stanimirova, T., Vergilov, I., Kirov, G. & Petrova, N. Thermal decomposition products of hydrotalcite-like compounds: Low-temperature metaphases. *J. Mater. Sci.* **34**, 4153–4161 (1999).
22. Ishihara, S. *et al.* Dynamic breathing of co2 by hydrotalcite. *J. Am. Chem. Soc.* **135**, 18040–18043 (2013).
23. Conterosito, E. *et al.* Facile preparation methods of hydrotalcite layered materials and their structural characterization by combined techniques. *Inorg. Chim. Acta* **470**, 36–50 (2018).
24. Artioli, G., Secco, M., Addis, A. & Bellotto, M. Role of hydrotalcite-type layered double hydroxides in delayed pozzolanic reactions and their bearing on mortar dating: Composition, Properties, Application. In *Cementitious Materials: Composition, Properties, Application* Vol. 500 (ed. Herbert, P.) (Walter de Gruyter GmbH, 2017).
25. Ricci, G. *et al.* The Cannero Castle (Italy): Development of radiocarbon dating methodologies in the framework of the layered double hydroxide mortars. *Radiocarbon* **62**, 617–632 (2020).
26. Boggs, S. J. & Krinsley, D. *Application of Cathodoluminescence Imaging to the Study of sedimentary Rocks* (Cambridge University Press, Cambridge, 2010).
27. Götze, J. Application of cathodoluminescence microscopy and spectroscopy in geosciences. *Microsc. Microanal.* **18**, 1270–1284 (2012).
28. Marshall, D. J. *Cathodoluminescence of Geological materials.* (1988).
29. Habermann, D., Newer, R. D. & Richter, D. K. Low limit of Mn2+-activated cathodoluminescence of calcite: State of the art. *Sedim. Geol.* **116**, 13–24 (1998).
30. Toffolo, M. B., Ricci, G., Caneve, L. & Kaplan-Ashiri, I. Luminescence reveals variations in local structural order of calcium carbonate polymorphs formed by different mechanisms. *Sci. Rep.* **9**, 7 (2019).
31. Toffolo, M. B., Ricci, G., Chapoulie, R., Caneve, L. & Kaplan-Ashiri, I. Cathodoluminescence and laser-induced fluorescence of calcium carbonate: A review of screening methods for radiocarbon dating of ancient lime mortars. *Radiocarbon* **62**, 545–564 (2020).
32. Richter, D. K., Götte, T., Götze, J. & Neuser, R. D. Progress in application of cathodoluminescence (CL) in sedimentary petrology. *Mineral. Petrol.* **79**, 127–166 (2003).
33. Hajdas, I. *et al.* Preparation and dating of mortar samples-mortar dating inter-comparison study (MODIS). *Radiocarbon* **59**, 1845–1858 (2017).
34. Artioli, G., Secco, M. & Addis, A. The vitruvian legacy: Mortars and binders before and after the Roman world. In *European Mineralogical Union Notes in Mineralogy* vol. 20, 151–202 (Mineralogical Society, 2019).
35. Ambers, J. Stable carbon isotope ratios and their relevance to the determination of accurate radiocarbon dates for lime mortars. *J. Archaeol. Sci.* **14**, 569–576 (1987).

36. Kosednar-Legenstein, B., Dietzel, M., Leis, A. & Stingl, K. Stable carbon and oxygen isotope investigation in historical lime mortar and plaster—Results from field and experimental study. *Appl. Geochem.* **23**, 2425–2437 (2008).
37. Strydonck, M. J., Dupas, M. & Keppens, E. Isotopic fractionation of oxygen and carbon in lime mortar under natural environmental conditions. *Radiocarbon* **31**, 610–618 (1989).
38. Addis, A. *et al.* New strategies for radiocarbon dating of mortars: Multi-step purification of the lime binder. In *4th Historic Mortars Conference - HMC 2016 10th-12th October 2016, Santorini, Greece,* 665–672 (2016).
39. Michalska, D. & Pawlyta, J. Modeled and measured carbon isotopic composition and petrographically estimated binder-aggregate ratio—Recipe for binding material dating?. *Radiocarbon* **61**, 799–815 (2019).
40. Zouridakis, N., Saliege, J. F., Person, A. & Filippakis, S. E. Radiocarbon dating of mortars from ancient Greek palaces. *Archaeometry* **29**, 60–68 (1987).
41. Dotsika, E., Psomiadis, D., Raco, B. & Gamaletsos, P. N. Isotopic analysis for degradation diagnosis of calcite matrix in mortar. *Anal. Bioanal. Chem.* **395**, 2227–2234 (2009).
42. Pachiaudi, C., Marechal, J., Strydonck, M. V., Dupas, M. & Dauchot-Dehon, M. Isotopic fractionation of carbon during $CO_2$ absorption by mortar. *Radiocarbon* **28**, 691–697 (1986).
43. Kim, S., Coplen, T. B. & Horita, J. Normalization of stable isotope data for carbonate minerals : Implementation of IUPAC guidelines. *Geochim. Cosmochim. Acta* **158**, 276–289 (2015).
44. Dietzel, M. Measurements of the stable carbon isotopes in calcite sinters on concrete. *ZKG Int.* **53**, 544–548 (2000).
45. Dietzel, M., Usdowski, E. & Hoefs, J. Chemical and 13C/12C- and 18O/16O-isotope evolution of alkaline drainage waters and the precipitation of calcite. *Appl. Geochem.* **7**, 177–184 (1992).
46. Létolle, R., Gégout, P., Rafai, N. & Revertegat, E. Stable isotopes of carbon and oxygen for the study of carbonation/decarbonation processes in concretes. *Cem. Concr. Res.* **22**, 235–240 (1992).
47. Usdowski, E. & Hirschfeld, A. The 13C/12C and 18O/16O composition of recent and historical calcite cement and kinetics of CO2 absorption by calcium hydroxide. *Neues Jahrb. Mineral. Monatshefte* **11**, 505–521 (2000).
48. Coplen, T. B. Reporting of stable hydrogen, carbon, and oxygen isotopic abundances (technical report). *Pure Appl. Chem.* **66**, 273–276 (1994).
49. Usdowski, E. & Hoefs, J. Oxygen isotope exchange between carbonic acid, bicarbonate, carbonate, and water: A re-examination of the data of McCrea (1950) and an expression for the overall partitioning of oxygen isotopes between the carbonate species and water. *Geochim. Cosmochim. Acta* **57**, 3815–3818 (1993).
50. Ergenç, D. & Fort, R. Multi-technical characterization of Roman mortars from Complutum, Spain. *Meas. J. Int. Meas. Confed.* **147**, 106876 (2019).
51. Eiler, J. & Schauble, E. 18O 13C 16O in Earth's atmosphere. *Geochim. Cosmochim. Acta* **68**, 4767–4777 (2004).
52. Lindroos, A., Ringbom, Å., Heinemeier, J., Hajdas, I. & Olsen, J. Delayed hardening and reactivation of binder calcite, common problems in radiocarbon dating of lime mortars. *Radiocarbon* **62**, 565–577 (2020).
53. Arslan, E. L'architettura romanica milanese. in *Storia di Milano, III. Dagli albori del Comune all'incoronazione di Federico Barbarossa (1002–1152),* 395–521 (1954).
54. Kingsley Porter, A. *Lombard Architecture, II.* (1916).
55. Segagni, A. Lomello. in *Enciclopedia dell' Arte Medievale* (1996).
56. Porter, K. A. *Lombard Architecture* (Hacker Art Books, 1967).
57. Stalley, R. *Early Medieval Architecture* (Oxford University Press, 1999).
58. Brogiolo, G. P., Chavvarìa, A. A., Giacomello, F. & Marinato, M. Scavi e ricerche 2013-2014 del complesso di Torba (VA). in *VI Congresso Nazionale degli Archeologi Medievisti Italiani, Lecce* (ed. Arthur, P.) 34–38 (2013).
59. Brogiolo, G. P. & Chavarría Arnau, A. *Torba (VA) – Scavi 2013–2019.* (Progetti di Archeologia, 2021).
60. Pistilli, A. Radiocarbon Dating Of Historical Mortars: Optimization Of The Binder Purification Protocol. (Università Degli Studi di Padova, 2016).
61. Vitruvio. *De Architettura, Book II, 4, 1.*
62. Dauzeres, A., Le Bescop, P., Sardini, P. & Cau Dit Coumes, C. Physico-chemical investigation of clayey/cement-based materials interaction in the context of geological waste disposal: Experimental approach and results. *Cem. Concr. Res.* **40**, 1327–1340 (2010).
63. Murakami, T., Hodgins, G. & Simon, A. W. Characterization of lime carbonates in plasters from Teotihuacan, Mexico: Preliminary results of cathodoluminescence and carbon isotope analyses. *J. Archaeol. Sci.* **40**, 960–970 (2013).
64. Dotsika, E., Lykoudis, S. & Poutoukis, D. Spatial distribution of the isotopic composition of precipitation and spring water in Greece. *Glob. Planet. Change* **71**, 141–149 (2010).
65. Fort, R., Ergenç, D., Aly, N., Alvarez de Buergo, M. & Hemeda, S. Implications of new mineral phases in the isotopic composition of Roman lime mortars at the Kom el-Dikka archaeological site in Egypt. *Constr. Build. Mater.* **268**, 121085 (2021).
66. Toffolo, M. B. & Boaretto, E. Nucleation of aragonite upon carbonation of calcium oxide and calcium hydroxide at ambient temperatures and pressures: A new indicator of fire-related human activities. *J. Archaeol. Sci.* **49**, 237–248 (2014).
67. Roosz, C. *et al.* Crystal structure of magnesium silicate hydrates (M-S-H): The relation with 2:1 Mg-Si phyllosilicates. *Cem. Concr. Res.* **73**, 228–237 (2015).
68. Bernard, E. Magnesium silicate hydrate (M-S-H) characterization: temperature, calcium, aluminum and alkali. *Phd thesis* (Université Bourgogne Franche-Comté, 2017).
69. Pesce, G. L. A. & Ball, R. J. Dating of Old Lime Based Mixtures with the "Pure Lime Lumps" Technique. In *Radiometric Dating* (ed. Nawrocka, D. M.) 21–38 (InTech, 2012). https://doi.org/10.5772/35419.
70. Brogiolo, G. Pietro. Il castello di Lomello. Aggiornamenti. In *Archeologia dei Longobardi. Dati e metodi per nuovi percorsi di analisi* (ed. Giostra, C.) 163–176 (Archeologia Barbarica 1, 2017).
71. Rietveld, H. M. A profile refinement method for nuclear and magnetic structures. *J. Appl. Crystallogr.* **2**, 65–71 (1969).
72. Gualtieri, A. F. Accuracy of XRPD QPA using the combined Rietveld-RIR method. *J. Appl. Crystallogr.* https://doi.org/10.1107/S002188989901643X (2000).
73. Ricci, G. *et al. New Strategies in Mortar Characterization and Radiocarbon Dating.*
74. Marzaioli, F. *et al.* Zinc reduction as an alternative method for AMS radiocarbon dating: Process optimization at CIRCE. *Radiocarbon* **50**, 139–149 (2008).
75. Terrasi, F. *et al.* High precision 14C AMS at CIRCE. *Nucl. Instrum. Methods Phys. Res. Sect. B Beam Interact. Mater. Atoms.* **266**, 2221–2224 (2008).
76. Bronk Ramsey, C. & Lee, S. Recent and planned developments of the program oxcal. *Radiocarbon* **55**, 720–731 (2013).
77. Reimer, P. J. *et al.* The IntCal20 northern hemisphere radiocarbon age calibration curve (0–55 cal kBP). *Radiocarbon* **62**, 725–757 (2020).

## Acknowledgements

## Author contributions

M.S., A.A., G.A. designed the research; A.A., M.S., A.P., I.P., N.P. collected data and performed laboratory work; G.R., M.S., A.A., N.P., F.M. analyzed and interpreted the data; G.P.B. and A.C.A. directed excavations, assembled and interpreted archaeological material; F.M., F.T., G.A. supervised laboratory work; G.R. drafted the manuscript, with contributions from all authors.

## Competing interests

The authors declare no competing interests.

## Additional information

**Supplementary Information** The online version contains supplementary material available at https://doi.org/ 10.1038/s41598-022-07406-x.

**Correspondence** and requests for materials should be addressed to G.R.

**Reprints and permissions information** is available at www.nature.com/reprints.

**Publisher's note** Springer Nature remains neutral with regard to jurisdictional claims in published maps and institutional affiliations.